Purinergic control of intercellular communication between Hensen's cells of the guinea-pig cochlea

Laura Lagostena*, Jonathan F. Ashmore†, Bechara Kachar‡ and Fabio Mammano*

**Settore di Biofisica e Istituto Nazionale di Fisica della Materia, Scuola Internazionale Superiore di Studi Avanzati (SISSA), 34014 Trieste, Italy, †Department of Physiology, University College London, Gower Street, London WC1E 6BT, UK and ‡Section on Structural Cell Biology, NIDCD, NIH, Bethesda, MD, USA*

(Received 1 July 2000; accepted after revision 9 November 2000)

1. Hensen's cells in the isolated cochlea were stimulated by extracellular adenosine 5′-triphosphate (ATP) applied to their endolymphatic surface while changes in membrane current and intracellular calcium concentration ($[Ca^{2+}]_i$) were measured simultaneously. The response consisted of (i) an initial rapid inward current accompanied by elevation of the $[Ca^{2+}]_i$, (ii) a more slowly rising inward current accompanied by a rise of the $[Ca^{2+}]_i$ and (iii) a slowly developing reduction of input conductance.

2. The slower responses were maintained in the absence of extracellular Ca^{2+}. Similar responses were produced by increasing the $[Ca^{2+}]_i$ via UV flash photolysis of intracellular D-myo-inositol 1,4,5-trisphosphate, P4(5)-(1-(2-nitrophenyl)ethyl) ester (caged InsP_3) loaded at pipette concentrations of 8–16 μM.

3. The slow inward current, reversing around 0 mV, was blocked by 4,4′-diisothiocyanatostilbene-2,2′-disulfonic acid (DIDS).

4. Bath application of U-73122 (1 μM), a phospholipase C inhibitor, eliminated the slow Ca^{2+}-release component of the response to ATP. It is proposed that the effects of ATP are mediated by the co-activation of ionotropic P2X and metabotropic P2Y receptors.

5. Immunohistochemistry using light and electron microscopy revealed that inositol 1,4,5-trisphosphate (InsP_3) receptors delineate a network within the cells.

6. The coupling ratio (CR) between cell pairs measured in dual patch-clamp recordings was 0.356 ± 0.024. The coupling reversibly decreased to 51% of the control within 2 min of applying 100 μM ATP. Flash photolysis of 32 μM intracellular caged InsP_3 and 1 mM caged Ca^{2+} reduced CR to 42 and 62% of the control, respectively.

7. We propose that endolymphatic ATP via P2X and P2Y receptors can control intercellular communication amongst Hensen's cells by reducing gap junction conductance in a Ca^{2+}- and InsP_3-dependent manner.

The supporting cells of the cochlea, Deiters' cells and Hensen's cells, that surround the sensory hair cells are joined through gap junctions (Kikuchi *et al.* 1995; Lautermann *et al.* 1998; Forge *et al.* 1999). They form an extensive syncitium that provides the basis for long-range electrical and metabolic cell-to-cell communication within the organ of Corti, the sensorineural epithelium of the cochlea (Fig. 1*A*). In addition it has been demonstrated that reversible dynamic structural changes can occur in Deiters' and Hensen's cells, together with a reversible reduction of the response sensitivity to test tones, following exposure to intense sound (Flock *et al.* 1999). The Hensen's cells are particularly prominent at the apex of the cochlea, where they are characterised by the presence of abundant lipid inclusions and mitochondria located near their lateral and apical membranes (Merchan *et al.* 1980). In Hensen's cells, gap junctions have been identified functionally by dye- and electrical-coupling patch-clamp experiments conducted in the whole organ of Corti (Mammano *et al.* 1996) as well as by *in vitro* and *in vivo* microelectrode recordings (Santos-Sacchi, 1987). Hensen's cells are adjacent to the outermost row of the outer hair cells, contact the basilar membrane and are highly permeable to K^+ (Mammano *et al.* 1996), the principal ion flowing through the mechano-sensory transduction channels of the hair cells. Hensen's cells may

thus be responsible for buffering K^+, collaborating in the maintenance of the cochlear fluid homeostasis (Wangemann & Schacht, 1996). This may be particularly significant in a structure like the organ of Corti, where 'spatial buffer' currents (Orkand, 1986) are likely to contribute to K^+ redistribution as the activity-related increase of extracellular K^+ promoted by propagation of travelling waves along the basilar membrane is highly non-uniform.

Sensory and supporting cells of the organ of Corti respond to extracellular application of nucleotides (Dulon *et al.* 1993; Sugasawa *et al.* 1996). The extracellular concentration of ATP can locally reach high values since this nucleotide can be secreted by various mechanisms (Dubyak & el Moatassim, 1993). In the organ of Corti, the distribution of P2X (ionotropic) and P2Y (metabotropic) purinoceptors suggests that purines may influence cochlear function at different sites. P2X and P2Y receptors, for example, are located at the apical (endolymphatic) pole of the outer hair cells. Such receptors are linked to an ATP-activated intracellular Ca^{2+} release cascade triggered by an InsP_3-gated intracellular store located at the base of the hair bundle (Mammano *et al.* 1999*b*). It is thought that $P2X_2$ receptor subunits in tissues lining the endolymphatic compartment of the cochlea mediate ATP-induced reduction in endocochlear potential. It has been proposed that such mechanisms could provide a protective role by decoupling the 'cochlear amplifier' in response to stressors, such as noise and ischaemia (Housley *et al.* 1999).

We describe here the Ca^{2+} signalling pathways and the membrane conductance changes of Hensen's cells associated with their purinergic activation within the organ of Corti *in situ*. We show by recording the currents in Hensen's cells during ATP application that the response can be characterised by three distinct components, one of which arises from direct cation influx through purinergic receptors and a second that can be identified as arising from InsP_3-mediated store release. By measuring coupling between cells, we identify alterations of gap junction conductance that follow from the elevation of intracellular calcium.

METHODS

Cell preparation

The preparation and methods of recording in the intact adult organ of Corti have been described previously (Mammano *et al.* 1996, 1999*b*). Adult guinea-pigs (200–400 g) were anaesthetised with chloroform and decapitated. All surgical and anaesthetic procedures used conformed with local and national guidelines. The temporal bones were removed from the skull and placed in a medium (artificial perilymph) containing (mM): NaCl, 137; KCl, 5.36; $CaCl_2$, 1.25; $MgCl_2$, 1.0; Na_2HPO_4, 1.0; KH_2PO_4, 0.44; $MgSO_4$, 0.81; at 4 °C. For some experiments, Ca^{2+} ions were excluded and the solution was supplemented by 2 mM EGTA (referred to as 0 $[Ca^{2+}]_o$ conditions in the text). pH was adjusted to 7.35 with NaOH and osmolarity to 320 ± 2 mosmol l^{-1} with D-glucose. Experiments were carried out at room temperature (24–26 °C).

Patch-clamp recordings

Conventional whole-cell patch-clamp recordings were made under visual control after mounting the recording chamber on a microscope stage (Fig. 1). List EPC-7 patch-clamp amplifiers (Heka Elektronik) were selected to record electrical signals using 1.5 mm o.d. soda glass (Harvard Apparatus). Current and voltage were sampled at rates between 1 and 20 kHz using a standard laboratory interface (1401Plus, Cambridge Electronic Design) controlled by customised software. Pipettes were filled with an intracellular solution containing (mM): KCl, 150; $MgCl_2$, 2.0; Na_2HPO_4, 8.0; NaH_2PO_4 1.0; Na_2ATP, 1.0; Na_2GTP, 0.3; adjusted to pH 7.2 with KOH and brought to 320 mosmol l^{-1} with D-glucose. For fluorescence imaging (see below), pipettes were filled with the cell-impermeable form of the Ca^{2+}-selective fluorescent dye Oregon Green 488 BAPTA-1 (100 μM, Molecular Probes) dissolved in the intracellular solution described above. Unlike Lucifer Yellow (Mammano *et al.* 1996) this dye did not spread across the patched cell boundary, consistent with the well-established property that pores within vertebrate cell-to-cell junctions exclude molecules larger than ~1 kDa. The pipette resistance was typically 1.5 MΩ when measured in the bath. No correction was applied to the data for liquid-junction potentials (estimated not to exceed −4 mV). Because of the low syncitial resistance (R_s; range 0.3–1.5 MΩ) and relatively low (uncompensated) pipette access resistance (R_a; range 2–4 MΩ) it proved impossible to apply *nominal* holding potentials that differed from their zero-current potential (V_0) by more than ±40 mV. After correction for the error due to the voltage drop across R_a, the *effective* holding potentials V_h ranged, in most cases, between −20 and +10 mV. ATP and other purinergic agonists were pressure applied through a patch pipette using a gated PicoPump (PV800, World Precision Instruments).

Ca^{2+} fluorescence imaging

Fluorescence imaging of intracellular Ca^{2+} was performed as described previously (Mammano *et al.* 1999*a*). Briefly, a narrow range of excitation wavelengths were selected around the absorption maximum (494 nm) of Oregon Green 488 BAPTA-1. Fluorescence emission was selected at 535 nm using a second filter set (XF23, Omega Optical) to form fluorescence images on a fast (15 MHz readout rate) CCD sensor (IA-D1, DALSA, Ontario, Canada) that was cooled by a Peltier device (Marlow Industries, Dallas, TX, USA). The sensor's output was digitised at 12 bits per pixel by customised electronics to produce 128 × 128 pixel images that were recorded in real time to the RAM of a host PC. The typical inter-frame interval for these recordings was between 8 and 16 ms. For each image pixel, fluorescence signals were computed as ratios $\Delta F/F_o = [F(t) - F(0)]/F(0)$, where t is time, $F(t)$ is fluorescence following a stimulus that causes calcium elevation within the cell and $F(0)$ is pre-stimulus fluorescence computed by averaging 10–20 images. Both $F(t)$ and $F(0)$ were corrected for mean background fluorescence computed from a 20 × 20 pixel rectangle devoid of obvious cellular structures. The fluorescence ratio magnitude was encoded by 8 bit pseudo-colour look-up tables to produce pseudo-colour images that were smoothed with a 3 × 3 pixel two-dimensional median filter.

UV flash photolysis of caged compounds

Flash photolysis of intracellular caged compounds was produced by the arc of a xenon flashlamp (JML-C2; Hi-Tech Sci. Ltd) coupled to the epifluorescence port of the microscope with a second light guide and a 45 deg dichroic mirror. The output of the guide was focused onto the organ of Corti via a pair of silica lenses (wavelengths approximately 300–400 nm) and a UVII bandpass filter. Adenosine-5′-triphosphate γ-(1-[2-nitrophenyl]ethyl) ester (caged ATP, 1 mM;

Sigma) was applied through pressure pipettes to the tissue as a continuous stream. The cell-impermeant forms of D-myo-inositol 1,4,5-trisphosphate, P4(5)-(1-(2-nitrophenyl)ethyl) ester (caged InsP_3, 8–32 μM; Molecular Probes) or of *o*-nitrophenyl EGTA (NP-EGTA, 2 mM; Molecular Probes) complexed with 1 mM Ca^{2+}, were loaded into selected cells through the patch pipette. The flash duration was estimated as $\leqslant$1 ms. Identical responses (to within 5%) of the ATP whole-cell current could be obtained on the same cell. No photobleaching of the Oregon Green 488 BAPTA-1 was detected either as a consequence of flash delivery or of illumination by the steady xenon source used to excite the dye.

Immunohistochemistry

Immunohistochemistry was performed as described in Mammano *et al.* (1999*b*). Briefly, guinea-pigs were killed by exposure to a rising concentration of carbon dioxide and decapitated, as dictated by NIH Guidelines for Animal Use. The bullae were opened and fixed in 4% paraformaldehyde in phosphate-buffered saline (PBS), pH 7.4, for 1 h. Samples were permeabilised with 0.5% Triton X-100 in PBS for 30 min, followed by overnight incubation in blocking solution (5% goat serum plus 2% bovine serum albumin in PBS). Samples were incubated with 2.5 μg ml^{-1} of a monoclonal antibody anti-InsP_3-receptor (cat. no. 407140; lot no. B25997; Calbiochem) for 1 h. A fluorescein isothiocyanate (FITC)-conjugate anti-mouse IgG (Amersham) was used as the secondary antibody. Samples were viewed with a confocal laser scanning microscope (Zeiss, Germany) equipped with a ×63 objective (NA = 1.4). No signal was detected when using the secondary antibody alone. For thin-section electron microscopy, organ of Corti samples were fixed using a reduced osmium method as described in Mammano *et al.* (1999*b*). For freeze-fracture, specimens were also prepared as described in Mammano *et al.* (1999*b*). Electron micrographs were taken with a Zeiss 902 electron microscope. For scanning electron microscopy, glutaraldehyde-fixed samples were critical-point dried, gold sputter coated and viewed in a Hitachi 4500 field emission scanning electron microscope (Hitachi, Japan).

RESULTS

Hensen's cells *in situ* reveal extensive electrical and dye-coupling that can be significantly reduced by the gap-junction blocker octanol applied in the bath at 1 mM (Mammano *et al.* 1996). In whole-cell recording conditions, Hensen's cells have a resting potential at depolarised zero-current values (V_0) of -6 ± 3 mV ($n = 105$) when bathed in octanol-free artificial perilymph, as previously described. In contrast, the average resting potential of Hensen's cells *in vivo* is −72 mV when recorded by sharp microelectrode recordings (Oesterle & Dallos, 1990). This difference can probably be ascribed to endolymph substitution with artificial perilymph at the apical surface of the organ of Corti that, under physiological conditions, is a strongly polarised epithelium (see Discussion).

Effect of ATP on membrane currents and intracellular Ca^{2+}

Hensen's cells were held under voltage clamp at a V_h in the range −15 to −10 mV, slightly more hyperpolarised than V_0. Because of the large syncitium conductance, the corresponding pre-stimulus offset currents were typically between −1 and −5 nA. Extracellular ATP applied from a pressure pipette (Fig. 1*C*) for 2 or 3 s evoked whole-cell currents that developed with a characteristic triphasic pattern. This pattern was characterised (i) by a large early inward deflection, followed (ii) by a second slower and smaller inward component and, at later times, (iii) by reduction of the pre-stimulus offset current (Fig. 2*A*, top). The calcium signal measured simultaneously showed a rapid rise at the endolymphatic pole of the cell (Fig. 2*A*, bottom, trace 1), spreading to the rest of the cytoplasm in ~3 s (traces 2 and 3). The same stimulation protocol was applied to construct the simultaneous dose–response curves at several ATP concentrations (from 3 to 200 μM). These are shown in Fig. 2*C*. Each point on these two plots is the average from three different cells. The data were fitted with the generalised logistic function:

$$y = [\mathrm{ATP}]^{n_H}/([\mathrm{ATP}]^{n_H} + K_A{}^{n_H}),$$

where the integer exponent n_H is the Hill coefficient and K_A is the half-activation concentration. Best least-square fits were obtained for Hill coefficients of 3, in both cases.

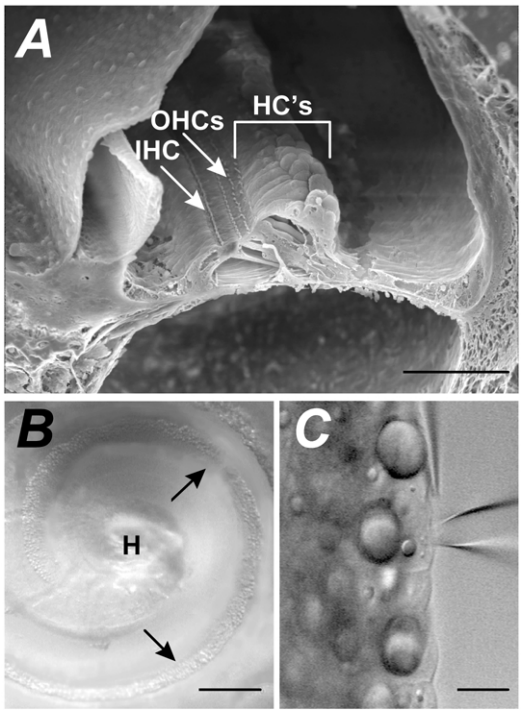

Figure 1. Hensen's cells *in situ*

A, sagittal section of the spiral canal in the apical turn of the guinea-pig cochlea showing sensory inner (IHC) and outer hair cells (OHCs) and radial extension of Hensen's cell region (HCs). *B*, video image of the apical turn in the isolated cochlea preparation (top view); H, helicotrema; arrows delimit the region studied in this paper. *C*, Hensen's cells, with prominent lipid inclusions. The patch pipette enters from the right whereas a thinner puff pipette, entering from the top, is positioned tangential to the tissue. Scale bars: *A*, 100 μm; *B*, 200 μm; *C*, 10 μm.

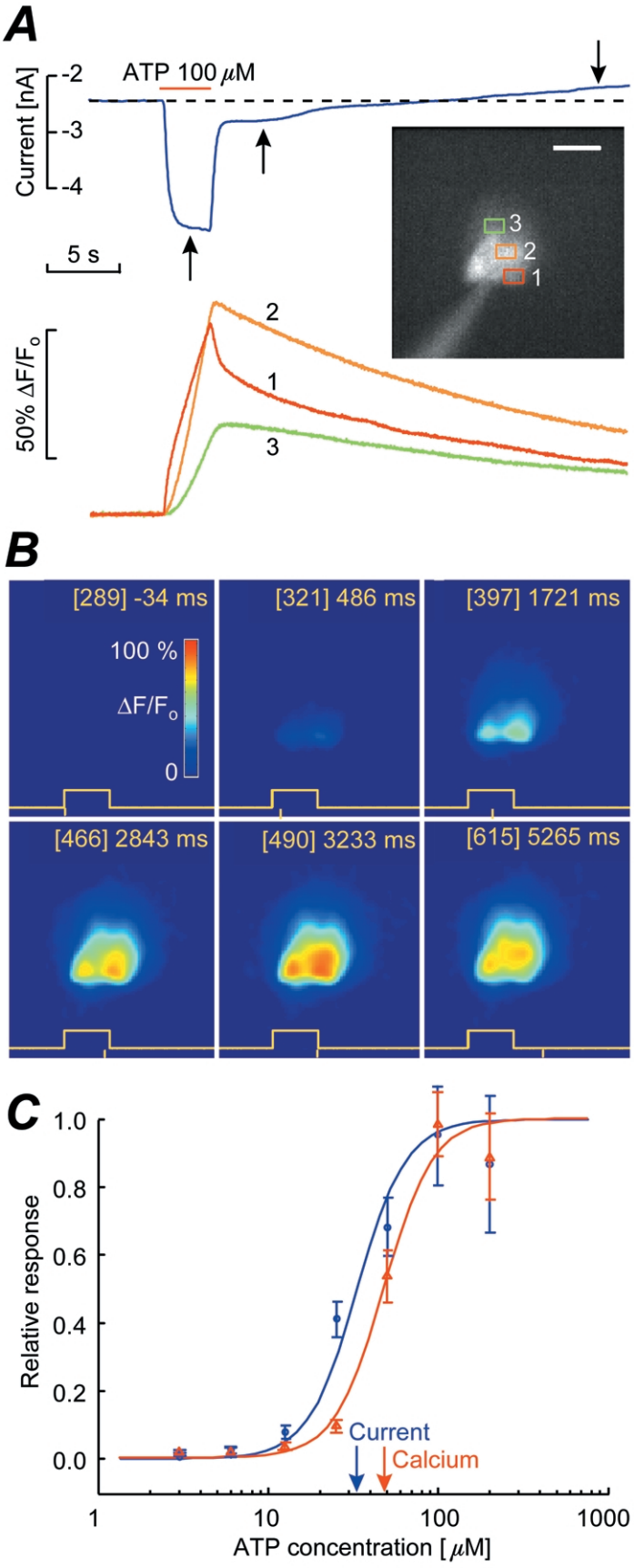

Figure 2. Effect of exogenous ATP

A, current and Ca^{2+} responses to pressure application of ATP (100 μM). Whole-cell current (top) where two distinct inward phases (i and ii, upward arrows) are followed by an outward phase (iii, downward arrow). Dashed line shows inward holding current. Oregon Green fluorescence responses (bottom) from number-coded regions of interest (ROIs) on cell image (inset; scale bar, 10 μm); each trace is the spatial average of the pixel signals from the corresponding ROI and was generated from a sequence of 2200 frames. Notice the faster rise of trace 1 at the endolymphatic pole of the cell. Cell holding potential $V_h = -11$ mV. *B*, six selected frames from the sequence. Times and sequential frame numbers (in square brackets) are also shown. The yellow trace at the bottom of each frame shows the timing of the ATP pulse and the relative timing of frame capture is marked by a vertical bar below this trace. The focal elevation of the $[Ca^{2+}]_i$ at the endolymphatic pole and propagating to the rest of the cytoplasm is evident. *C*, ATP dose–response curve. Each point is the average of 3 cells: circles, peak inward current; triangles, peak Ca^{2+} response, measured at the endolymphatic pole; continuous lines through data are non-linear Levenberg-Marquardt fits (see text).

However, K_A for current, $K_A(I_{ATP})$, equalled 33.1 ± 1.7 μM ($n = 3$) whereas K_A for Ca^{2+}, $K_A(Ca^{2+})$, equalled 47.9 ± 1.2 μM ($n = 3$). The difference between $K_A(I_{ATP})$ and $K_A(Ca^{2+})$ was statistically significant ($P < 0.02$), suggesting either the involvement of receptors with different affinities for ATP and/or Ca^{2+} buffering in the cytoplasm. The late inward components and the reduction of the pre-stimulus offset current were not evoked by short duration pulses (< 100 ms) of ATP at a concentration $< K_A(Ca^{2+})$.

Effects of purinergic antagonists and agonists

To investigate the type of purinoceptors present on Hensen's cells, pyridoxalphosphate-6-azophenyl-2′,4′-disulfonic acid (PPADS, 30 μM), a selective antagonist to P2 purinoceptors, was added to the superfusate. In two cells, responses to 30 μM ATP were tested and found before introduction of PPADS. Within 5 min, both current and Ca^{2+} responses to ATP were completely suppressed. Cells did not recover for up to 40 min. To discriminate amongst different subtypes of P2 purinoceptors we performed experiments in which the current evoked by a brief ATP application (30 μM, 50 ms) was compared with the currents elicited by the presumed P2Y receptor agonist 2-methylthio-ATP (2-meSATP), applied at 30 μM and 1 mM. Only the rapid inward current was activated by ATP and by 2-meSATP (the latter with > 5-fold different potency). The relatively large value of K_A commanded the investigation of whether $P2Z/P2X_7$ receptors, which are known to bind ATP with low affinity (~300 μM), were involved in the responses. The selective agonist 2′- and 3′-*O*-(4-benzoybenzoyl)-ATP (BzATP) that acts on these receptors with 5-fold larger potency than ATP (Chessel *et al.* 1997), was completely ineffective up to 1 mM, a saturating concentration (data not shown).

Spatial and temporal characteristics of the ATP-induced Ca^{2+} response

To obtain a rapid application of ATP, pressure-applied extracellular caged ATP (1 mM) was directed onto the tissue as a continuous stream. A focused 1 ms UV flash was delivered through the microscope objective to produce an [ATP] jump that, compared with puff application of ATP, resulted in a response that was not diffusion limited (Fig. 3*A*). Flash photolysis also shortened the exposure of the cell to the agonist's active form, enabling the intrinsic signal dynamics to be

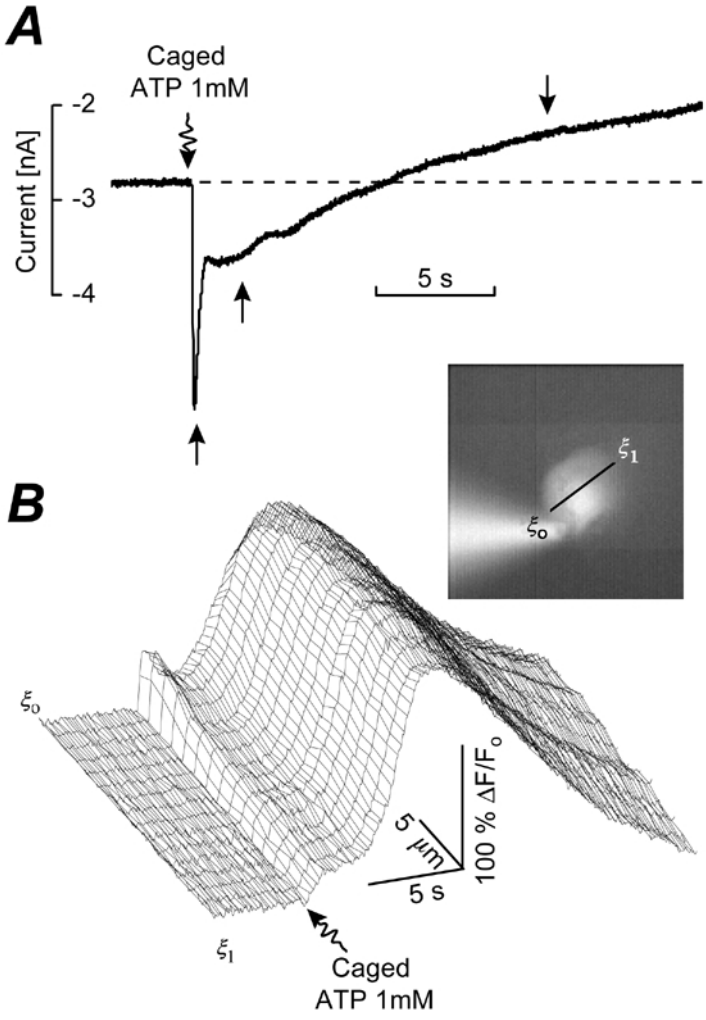

Figure 3. UV photolysis of exogenous caged ATP

A, a continuous stream of caged ATP (1 mM) ejected from the puff pipette was illuminated by a UV flash (300–400 nm, 1 ms, curly arrow). Whole-cell current trace shows two inward phases (i) and (ii) (upward arrows) and an outward phase (iii) (downward arrow). Pre-stimulus offset current is shown as dashed line. *B*, space–time plot of Oregon Green fluorescence. The fluorescence was measured along a 20 μm line ξ_0–ξ_1 superimposed on the cell's medial axis shown in the inset. Abscissa is time; surface height gives local fluorescence change. Notice biphasic Ca^{2+} response with a rapid first peak, corresponding to Ca^{2+} entry and localised near ξ_0, and a second larger peak forming simultaneously at all locations along ξ_0–ξ_1. *A* and *B* are from two different cells, both held at $V_h = -11$ mV.

detected with improved resolution. However, the initial inward current (phase i) was of much shorter duration.

Following the UV flash, the $[Ca^{2+}]_i$ increased in a biphasic manner: a concentration gradient was rapidly established with the highest levels initially formed at the endolymphatic cell pole. Progressively $[Ca^{2+}]_i$ increased throughout the cytoplasm (Fig. 3*B*). The delayed Ca^{2+} signal was severalfold greater than the initial signal and reached a maximum at 4.2 ± 0.7 s after the flash. Levels returned to baseline with a time constant of 11.2 ± 1.3 s ($n = 10$).

These results collectively indicate that the activation of Ca^{2+}-permeable ionotropic P2X receptors are responsible for the first response peak and strongly suggest that second messenger systems, contributing to the elevation of the $[Ca^{2+}]_i$, are responsible for the later and slower peaks.

Effect of extracellular Ca^{2+} removal

To investigate release from intracellular stores, ATP was transiently applied to Hensen's cells in Ca^{2+}-free extracellular medium (Fig. 4). In 0 $[Ca^{2+}]_o$, the three distinct response phases of the whole-cell current were clearly separated (Fig. 4*A*, top). The first rapid peak of Ca^{2+} response was absent, although $[Ca^{2+}]_i$ continued to rise simultaneously throughout the cell (Fig. 4*B*, bottom). The time course of the Ca^{2+} signal resembled closely the rise and fall of the slower response observed in the presence of standard 1.25 mM $[Ca^{2+}]_o$. The $[Ca^{2+}]_i$ peaked 3.8 ± 1.1 s after flash delivery, returning to the baseline with a time constant of 12.3 ± 1.8 s ($n = 6$). From Fig. 4*A*, it is clear that the secondary inward current (phase (ii)) peaked when the $[Ca^{2+}]_i$ was approaching its maximum, suggesting that it may have been due to a Ca^{2+}-dependent conductance change. The frame sequence of Fig. 4*B* also shows that no concentration gradient formed within the

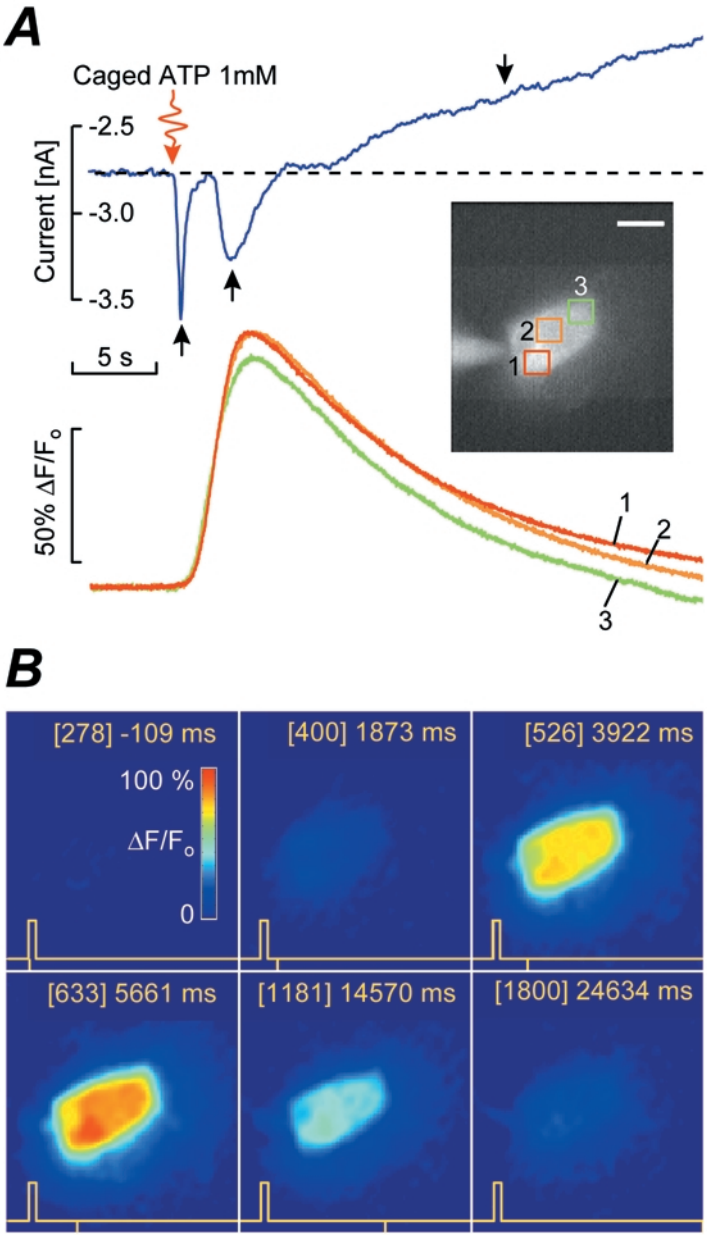

Figure 4. ATP responses in 0 $[Ca^{2+}]_o$

A, top: whole-cell current elicited by the UV photolysis of 1 mM caged ATP (curly arrow). Two inward phases (i) and (ii) (upward arrows) with markedly distinct onsets are followed by a prominent outward phase (iii) (downward arrow) relative to holding current; inset: fluorescence image of the patched cell with 3 superimposed colour- and number-coded ROIs (scale bar, 10 μm); bottom: Ca^{2+} fluorescence traces from the corresponding ROIs in *A*. The early phase and simultaneous non-uniform rise of the signal at all 3 locations is apparent. *B*, six images from the sequence used in *A*, captured at the times shown. Timing as in Fig. 2. Holding potential $V_h = -12$ mV.

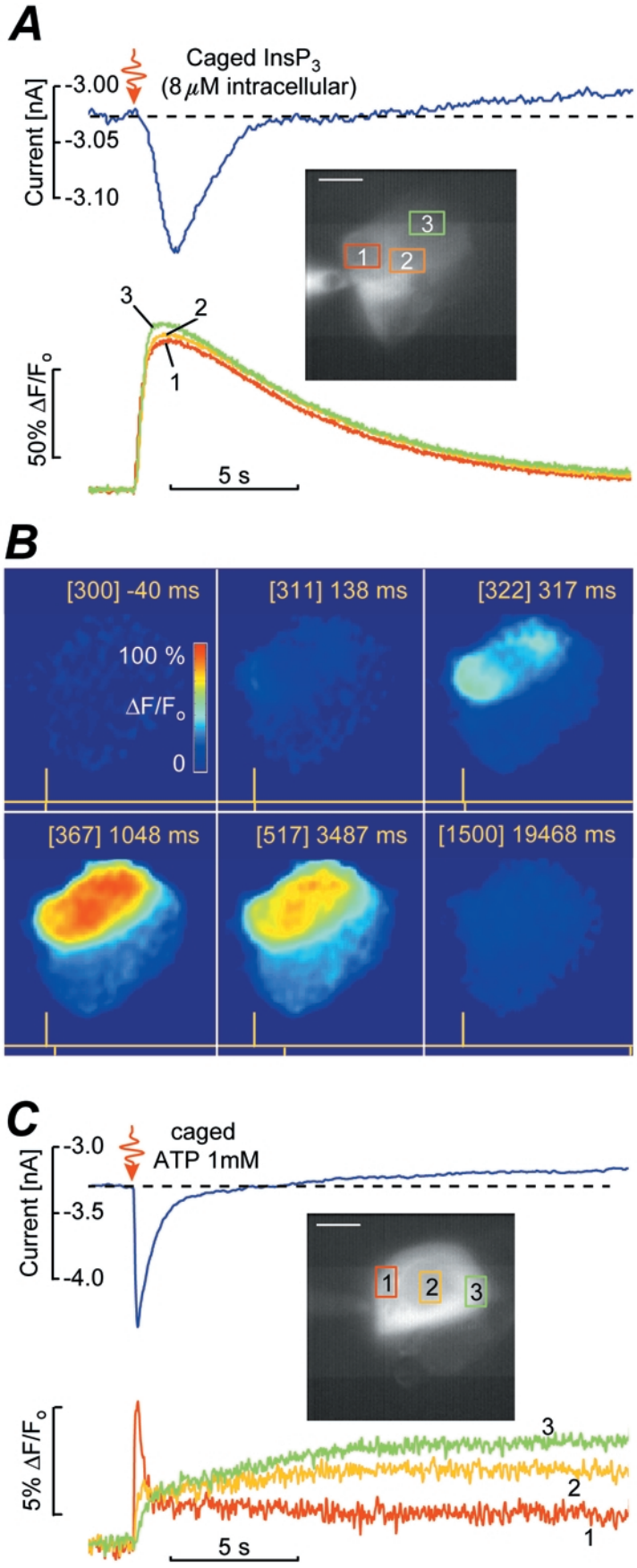

Figure 5. UV photolysis of intracellular caged InsP_3 and its inhibition by U-73122

A, top: whole-cell current elicited by 1 ms UV flash (curly arrow) in a cell loaded with 8 μM caged InsP_3 through the patch pipette; inset: fluorescence image of the patched cell with 3 superimposed colour- and number-coded ROIs; scale bar: 10 μm; bottom: Ca^{2+} fluorescence from the corresponding ROIs in inset. Note simultaneous signal rise at all locations. *B*, six selected images from the sequence used in *A*, captured at the times shown; timing notation as in Fig. 2. The presence of a second cell, in this case dye-coupled to the patched cell, is evident as a faint halo surrounding the dye-filled cell; holding potential $V_h = -12$ mV. *C*, effect of the phospholipase C inhibitor U-73122. Top: whole-cell current evoked by the UV photolysis of caged 1 mM ATP (curly arrow); bottom: simultaneous fluorescence signals sampled from the corresponding ROIs, labelled 1–3, superimposed on the cell image (inset). In the presence of the inhibitor there was no delayed inward phase in the current response and no delayed component in Ca^{2+} rise (compare with Fig. 3); holding potential, $V_h = -10$ mV.

cell cytoplasm. This would be consistent with the absence of any Ca^{2+} entry from the endolymphatic surface of the cell (compare to Fig. 2*B*).

Effects of intracellular InsP_3 and inhibition of phospholipase C

Metabotropic P2Y ATP receptors mobilise intracellular Ca^{2+} by activating phosphoinositide-specific PLC, an enzyme that hydrolyses phosphatidylinositol 4,5-bis-phosphate into InsP_3 and diacylglycerol (Linden, 1999). To provide evidence for a second messenger coupled purinoceptor in Hensen's cells we loaded the cytoplasm of Hensen's cells with caged InsP_3 (8–16 μM) through the patch pipette (Fig. 5). Representative responses evoked by the UV photolysis of this membrane-impermeant compound are shown in Fig. 5*A* and *B*. Similar results were obtained in two other cells. The InsP_3-evoked current (Fig. 5*A*, top) was biphasic, lacking the early inward component (which, based on the blocking effect of pyridoxalphosphate-6-azophenyl-2,4-disulphonic acid (PPADS), is due to cation influx following the activation of P2X receptors). Comparison with Figs 3*A* and 4*A* indicates that the current components activated by intracellular InsP_3 corresponded to the delayed inward phase (phase (ii)) and reduction of the pre-stimulus offset current (phase (iii)) elicited by application of extracellular ATP. Ca^{2+} fluorescence evoked by InsP_3 increased synchronously throughout the cytoplasm (Fig. 5*A*, bottom), as occurred in 0 $[Ca^{2+}]_o$.

The sequence of frames in Fig. 5*B* highlights the uniform fluorescence change evoked by InsP_3. Bath application of U-73122 (1 μM), a PLC inhibitor (Venance *et al.* 1997), reduced the Ca^{2+} response evoked by UV photolysis of extracellular caged ATP (1 mM) to a monophasic rise

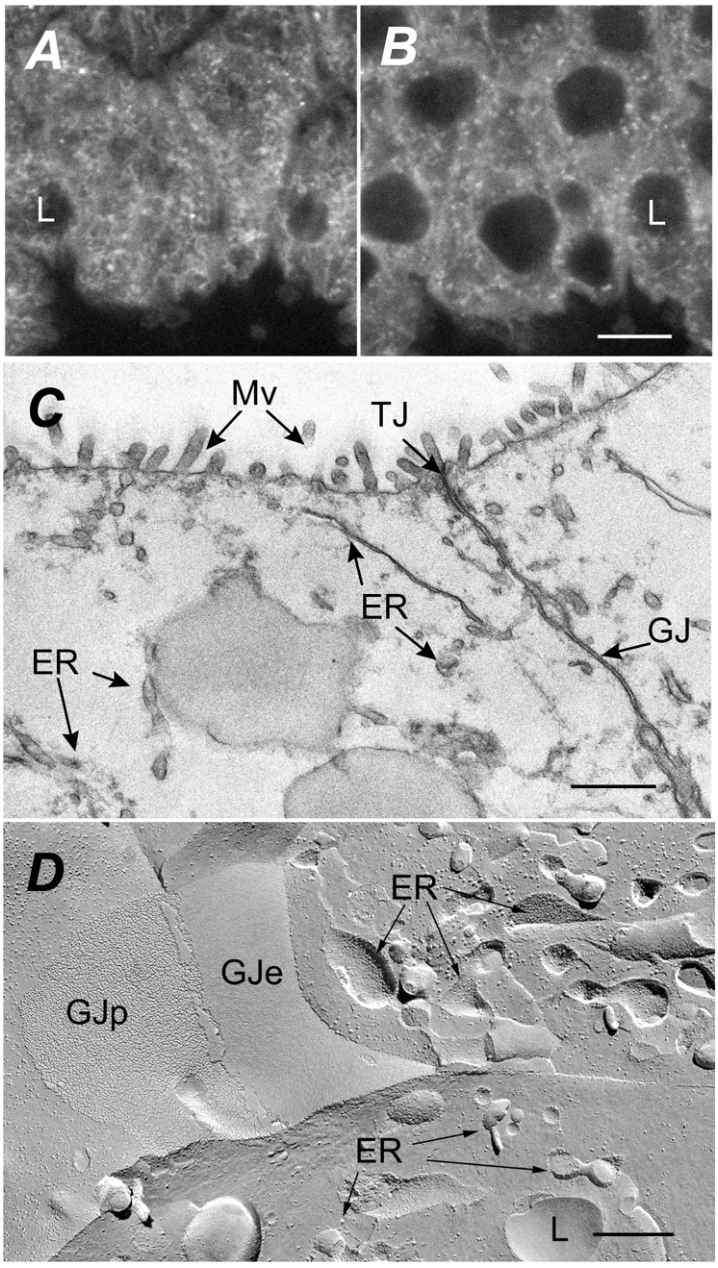

Figure 6. Immunolocalisation of InsP_3 receptors and electron microscopy of Hensen's cells

A and *B*, confocal microscopy ~0.8 μm cross-sections at 2 (*A*) and 15 μm (*B*) below the apical surface of the Hensen's cells from a whole mount preparation of the organ of Corti, labelled with the anti-InsP_3 receptor antibody. Punctuate and trabecular patterns of fluorescence are seen throughout the whole cytoplasm; L, lipid inclusions. *C*, thin section electron microscopy of the apical region of two neighbouring Hensen's cells showing the vesicular and trabecular endoplasmic reticulum (ER) dispersed throughout the cytoplasm; GJ, gap junctions; TJ, tight junctions; Mv, microvilli. *D*, freeze-fracture replica of a region of contact between two adjacent Hensen's cells showing a large gap junction plaque between their contacting plasma membranes. GJp indicates the cluster of connexons viewed on the protoplasmic fracture face of the plasma membrane, and GJe indicates a view of the characteristic pits left of the exoplasmic fracture face of the adjacent plasma membrane. ER, endoplasmic reticulum membranes; L, lipid inclusion. Scale bars: *A* and *B*, 5 μm; *C* and *D*, 1 μm.

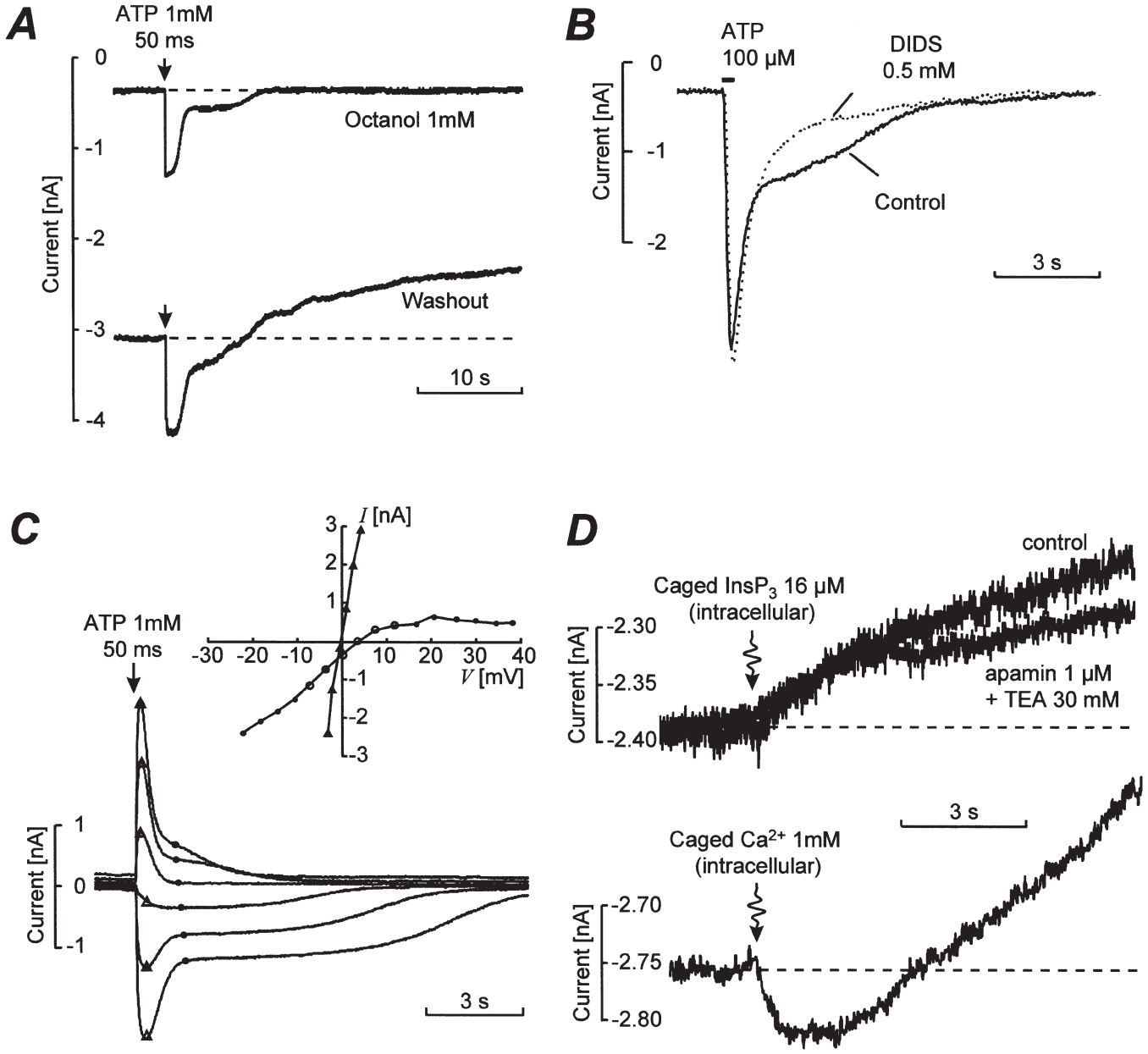

Figure 7. Ca^{2+} activation of inward and outward phases of the whole-cell current

A, response to pressure application of 1 mM ATP (50 ms; arrows) from a cell bathed in octanol (1 mM, top trace); and 15 min after octanol washout. Holding potential $V_h = -18$ mV. *B*, continuous line: control response to a puff application of ATP (100 μM, 100 ms; horizontal bar) in the presence of 1 mM octanol; dotted line: response obtained from the same cell, after adding the selective Cl^- channel blocker DIDS (0.5 mM) to the superfusate for 5 min; $V_h = -18$ mV; *C*, whole-cell currents evoked by ATP (1 mM, 50 ms) at 6 different command potentials around 0 mV in the presence of 1 mM octanol. Triangles and circles indicate current values on the corresponding current–voltage (*I–V*) plots, shown as an inset. To construct the *I–V* plots, leakage currents were estimated from the trace fraction preceding ATP application, currents were leak-subtracted and voltages were corrected for the error due to the access resistance (3.12 MΩ). *D*, top: activation of the outward phase response by UV photolysis of intracellular caged $InsP_3$ (16 μM) in the presence of 0.5 mM DIDS. A 1 ms flash (curly arrow) was applied before (control) and after introducing saturating concentrations of the Ca^{2+}-activated K^+ channel blockers TEA (30 mM) and apamin (1 μM) in the superfusate; $V_h = -12$ mV; bottom: whole-cell current evoked by 1 ms UV flash (curly arrow), photolysing a mixture of 2 mM NP-EGTA complexed with 1 mM caged Ca^{2+} loaded through the patch pipette; notice biphasic response; $V_h = -10$ mV.

(Fig. 5*C*). The fluorescence increased rapidly at the cell's apical pole, where it was maximal (trace 1), and augmented with progressively larger delays proceeding from the apical to the basal cell pole (traces 2 and 3). This indicates that Ca^{2+} entered the endolymphatic cell boundary and diffused through the cytoplasm. In contrast to the controls in Fig. 3, a delayed and prominent Ca^{2+} elevation, typical of cells with a functional InsP_3 pathway, was not present in any of the three cells tested. The whole-cell current lacked the delayed inward phase, whereas the delayed reduction of the pre-stimulus offset current was present in two cells. Together, the results in Fig. 5 strongly support the notion of a PLC-linked InsP_3-dependent transduction pathway in the ATP-evoked responses of Hensen's cells.

Immunohistochemistry

We observed that InsP_3 receptors were expressed throughout the cytoplasm of Hensen's cells (Fig. 6*A* and *B*), where the labelling produced by monoclonal anti-InsP_3 receptor antibodies appeared as a punctuated and segmented pattern. Electron microscopy (Fig. 6*C*) and the freeze-fracture replica (Fig. 6*D*) provides further evidence for the intracellular stores likely to be responsible for the Ca^{2+} release. The putative release sites are located at the vesicular and trabecular endoplasmic reticulum (ER) dispersed throughout the cytoplasm.

Late currents induced by ATP

In the presence of 1 mM octanol the holding currents of the cell were considerably reduced and the late component of the response was not elicited by the puff applications of ATP. In Fig. 7*A* an experiment is shown where a cell was held at −15 mV while bathed in octanol (1 mM) and stimulated by ATP (1 mM, 50 ms). The ATP elicited only a fast and a delayed inward current. Upon switching to the standard (octanol-free) bathing medium (bottom trace), the inward offset current (dashed line) increased to several nanoamps. The simplest explanation is that current is then allowed to flow through gap junctions into the coupled cellular network.

Figure 7*B* shows the response of an octanol-bathed Hensen's cell to ATP before (control, continuous line) and after the introduction of DIDS (0.5 mM, dotted trace) a selective and irreversible anion channel inhibitor (Hille, 1992). While the early phase of the response was unaffected, the delayed inward component was suppressed by DIDS. This suggests that the delayed inward current was due to a Ca^{2+}-activated Cl^- conductance.

To characterise the voltage dependence of this conductance, we repeatedly applied ATP puffs (1 mM, 50 ms) at 1 min intervals to an octanol-bathed cell held at

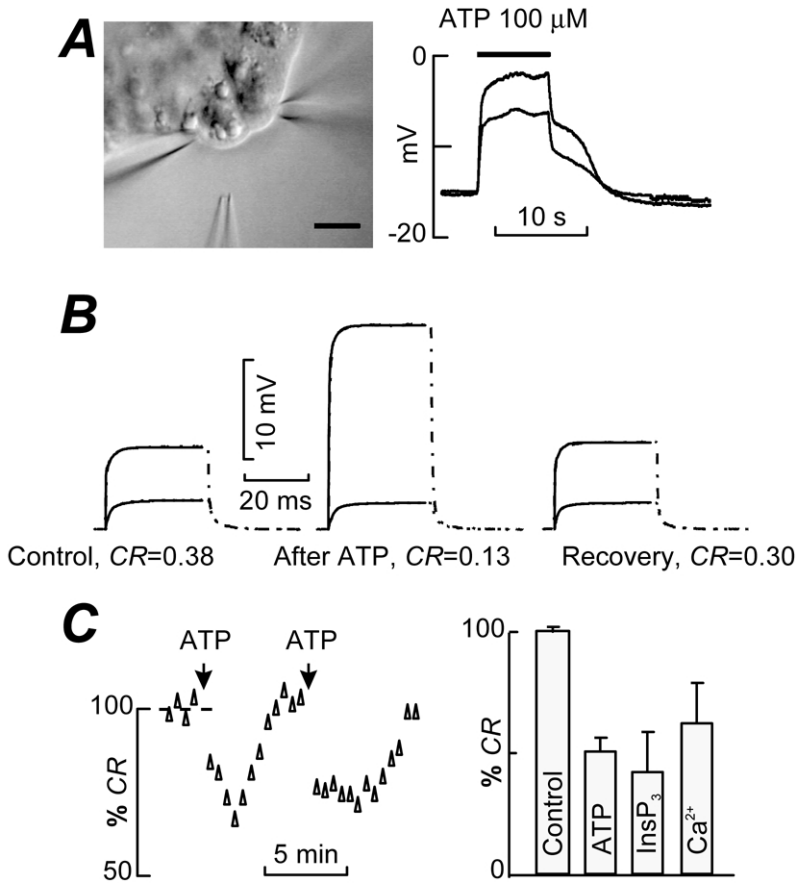

Figure 8. Control of electrical coupling by ATP, InsP_3 and $[Ca^{2+}]_i$

A, voltage responses evoked by ATP from the double patched cells both held under current clamp. Scale bar: 10 μm. *B*, voltage responses evoked in a cell pair by injecting current into one (250 pA, 43 ms) to measure coupling ratios (CR) before (left traces, control), 2 min (middle traces) and 5 min (right traces, recovery) after puffing 100 μM ATP for 8 s; continuous lines superimposed on voltage recordings (dashed and dotted lines) are saturating double-exponential non-linear Levenberg-Marquardt fits. *C*, left: time course of the percentage CR, normalised to the mean of the pre-stimulus values (dashed line); arrows indicate pressure application of ATP (100 μM, 8 s); right: pooled data showing percentage CR normalised to their respective pre-stimulus mean values (see text). ATP applied focally by pressure (100 μM, 8 s) reduced CR to 51 ± 6 % of the control within 2 min ($n = 9$ pairs); flash photolysis of intracellular caged InsP_3 (32 μM) and caged Ca^{2+} (1 mM) reduced CR to 42 ± 16 % ($n = 4$ pairs) and 62 ± 11 % ($n = 3$ pairs), respectively. Time-dependent recordings in *A*–*C* are from different cell pairs.

different potentials (V_h) in the range −25 to +40 mV. Representative current traces, elicited by ATP at six such potentials around 0 mV, near the expected equilibrium potential for Cl^- (0.1 mV), are displayed in Fig. 7*C*. Both currents reversed close to 0 mV. In the range of potentials tested, the early response showed no appreciable rectification. In contrast, the Ca^{2+}-activated Cl^- current deviated appreciably from linearity at positive potentials. The behaviour of the *I–V* relationship may have been due either to an intrinsic inward rectification of the channel or to a decreased contribution from extracellular Ca^{2+} entry at depolarised potentials (or both). Two out of two other cells produced results similar to those in panels *B* and *C*.

In an epithelial cell line, extracellular ATP mobilises intracellular Ca^{2+} activating both Cl^- and K^+ currents (Nilius *et al.* 1995). Ca^{2+}-activated K^+ channels promote the outward flow of K^+ down its electrochemical gradient and are generally blocked either by low millimolar extracellular TEA, or by apamin at sub-micromolar concentrations (Hille, 1992). The delayed phase of the ATP-evoked current that appears as an outward current relative to the pre-stimulus offset current was selectively activated by flash photolysis of intracellular caged InsP_3 (16 μM) in the presence of 0.5 mM DIDS to suppress the Ca^{2+}-activated Cl^- conductance. However, the response to InsP_3 was not suppressed either by 30 mM TEA or by 1 μM apamin (Fig. 7*D*, top). We conclude that this component of the ATP-evoked response is not an outward current arising from the activation of Ca^{2+}-dependent ion channels but instead a consequence of a *decrease* of the network input conductance.

Olfactory receptor neurones possess non-specific cation and Ca^{2+}-permeable channels that are directly gated by InsP_3 and that display similarities to the InsP_3-gated channels found in the membranes of intracellular stores (Lischka *et al.* 1999). To discriminate between a direct and indirect (Ca^{2+}-mediated) action of InsP_3, we used UV flash photolysis of the photolabile Ca^{2+} chelator NP-EGTA (2 mM) complexed to Ca^{2+} (1 mM) and loaded into selected Hensen's cells through the patch pipette. The results in Fig. 7*D* (bottom) support the conclusion that the current responses in Figs 5*A* and 7*D* (top) are generated by InsP_3 indirectly, through increased levels of the $[Ca^{2+}]_i$ caused by release from intracellular stores. In summary, the results in Fig. 7 indicate that the delayed inward phase of the ATP-evoked current was due to the activation of a Ca^{2+}-dependent Cl^- conductance, possibly mediated by Cl^- channels present on the endolymphatic surface of the Hensen's cell membrane (Ashmore & Balme, 1988; Sugasawa *et al.* 1996). In contrast, the delayed decrease of the pre-stimulus offset current most probably resulted from the Ca^{2+}-dependent down-regulation of gap junction permeability.

Effect of ATP, InsP_3 and Ca^{2+} on the coupling ratio of Hensen's cells

It is known that gap junction communication is affected by the $[Ca^{2+}]_i$ (Rose *et al.* 1977). To measure coupling ratios, pairs of Hensen's cells were patch-clamped using pipettes loaded with 100 μM Oregon Green 488 BAPTA-1. The voltage responses of both cells (1 and 2) were acquired when current pulses in the range 100–480 pA were injected into cell 1. The coupling ratio, CR, was computed as:

$$CR = \Delta V^{ss}{}_2 / \Delta V^{ss}{}_1,$$

where $\Delta V^{ss}{}_i$ $(i = 1,2)$ indicates the steady voltage responses. For cells less than 50 μm apart, the coupling

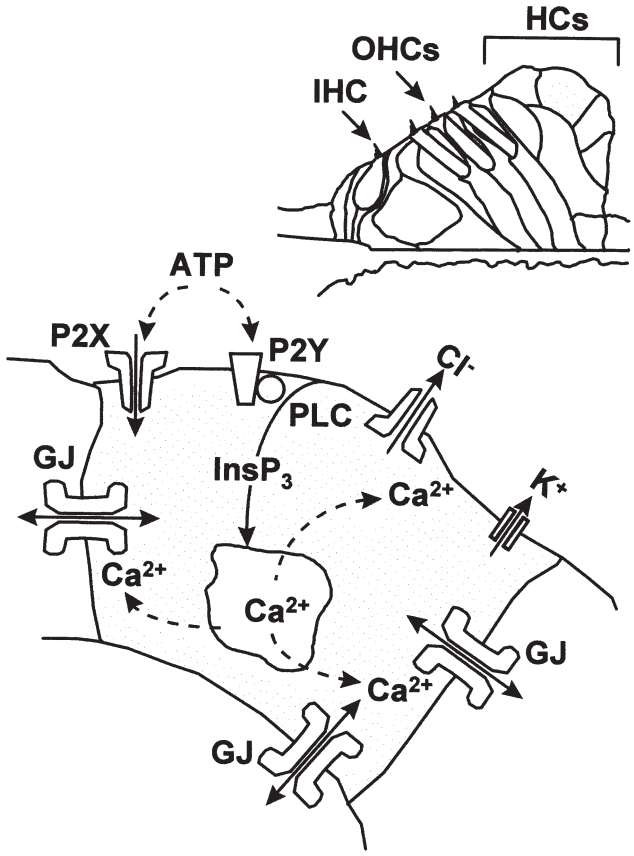

Figure 9. Scheme for the effect of ATP on Hensen's cells

Binding to P2X receptors promotes influx of cations, including Ca^{2+}, whereas binding to P2Y receptors activates phospholipase C (PLC) and produces InsP_3, which in turn causes the release of Ca^{2+} from intracellular stores. Raised Ca^{2+} levels within the cytoplasm favour the opening of Ca^{2+}-activated Cl^- channels at the cell endolymphatic pole, where a small K^+ conductance is also present. Ca^{2+} acts also on gap junctions (GJ) that interconnect supporting cells in the organ of Corti. IHC, inner hair cell; OHCs, outer hair cells; HCs, Hensen's cells.

ratio CR was 0.356 ± 0.024 ($n = 18$ pairs). Focal pressure application of ATP (100 μM, 8 s) evoked similar voltage responses in both cells held under current clamp (Fig. 8*A*). We monitored CR before and after the pressure application of ATP (Fig. 8*B*) and found that it decreased reversibly as the input conductance of the current-injected cell transiently increased (middle traces). The effects of ATP were highly reproducible over stable recordings of tens of minutes. ATP reduced CR to 51 ± 6 % of the control ($n = 9$ pairs), whereas UV flash photolysis of intracellular caged InsP_3 (32 μM) and caged Ca^{2+} (1 mM) reduced it to 42 ± 16 % ($n = 4$ pairs) and 62 ± 11 % ($n = 9$ pairs), respectively (Fig. 8*C*, right).

DISCUSSION

Regulation of cochlear sensitivity by purines

In vivo experiments have demonstrated that when ATP is introduced into the endolymphatic fluid compartment of the cochlea, there is a dose-dependent reduction in the endocochlear potential and cochlear microphonics (Muñoz *et al.* 1999) as well as in evoked emissions (Kirk & Yates, 1998). It has also been proposed that the extracellular concentration of ATP increases after tissue injury (Dulon *et al.* 1993) and that ATP release in a calcium-dependent manner occurs from cochlear tissues (Wangemann, 1996). A specific source of such endolymphatic purine compounds has been identified in a region of the marginal cells of the stria vascularis (White *et al.* 1995). Recently, it has also been shown that ATP is released in cochlear fluids as a consequence of increasing sound levels, with reported concentrations in the sub-micromolar range (Thorne *et al.* 1999) whereas we found a half-activation concentration of ~33 μM. This discrepancy indicates that there may be as yet uncharacterised mechanisms that produce a much higher concentration of ATP at the endolymphatic surface of the Hensen's cells. It is also possible that the high ecto-ATPase activity in the scala media (Vlajkovic *et al.* 1998) may have contributed significantly to biasing the measurement of the sound-evoked increase of [ATP] to unrealistically low levels. Finally, the K_A we found may be an overestimate of the effective value in endolymph since ATP would have been buffered in our extracellular medium by divalent cations such as Ca^{2+} and Mg^{2+} (Cockcroft & Gomperts, 1979).

We have recently shown that the action of ATP on sensory outer hair cells of the guinea-pig cochlea involves rapid changes in the intracellular concentration of Ca^{2+} at the cell's apical pole (Mammano *et al.* 1999*b*). That sensory and supporting cells respond to the same external chemical stimuli is consistent with immunolabelling studies for a high density of $P2X_2$ receptor subunits have been found on the apical aspect of the stereocilia of the inner and outer hair cells and on the endolymphatic surface of Hensen's cells and third row Deiters' cell processes (Housley *et al.* 1999). However, our data indicate that Hensen's cell responses to ATP depend also on the activation of a Ca^{2+}-mobilising intracellular cascade promoted by the activation of metabotropic P2Y ATP receptors. Furthermore, the whole-cell current response in Hensen's cells exhibits a more complex behaviour than in outer hair cells, developing two additional phases provided that the concentration of ATP reaches a critical level (above about 40 μM) for a sufficient time interval (greater than 50 ms). These inward and outward response phases activated by ATP represent modulation of the Hensen's cell permeability both to Cl^- and to intercellular communication (Fig. 9).

Control of Cl^- permeability

In other epithelia, ATP has been shown to induce a release of Ca^{2+} from intracellular stores and thereby gate Ca^{2+}-activated ion currents, especially Cl^- currents (Nilius *et al.* 1995). The signalling pathway that underlies the modulation of Hensen's cell Cl^- permeability by ATP shares many features with other sensory systems. For instance, a Ca^{2+}-dependent Cl^- conductance participates directly in vertebrate olfactory transduction (Kurahashi & Yau, 1993). In cells from the retinal pigment epithelium, rich in transport proteins that allow it to mediate the vectorial movement of metabolite ions and fluid, ATP-dependent elevation of the $[Ca^{2+}]_i$ by InsP_3 leads to activation of Cl^- channels involving cytosolic Ca^{2+} stores, as well as Ca^{2+} influx from extracellular space (Strauss *et al.* 1999).

In the above experiments, a delayed inward current caused by increased Cl^- permeability was triggered both by application of ATP in 0 $[Ca^{2+}]_o$ and by UV photolysis of intracellular caged InsP_3. In contrast, the Cl^- conductance described by Sugasawa *et al.* (1996) in clusters of dissociated Hensen's cells was Ca^{2+} activated secondarily to Ca^{2+} influx, since it required the presence of extracellular Ca^{2+}. This difference may be ascribed to damage caused to the InsP_3-dependent cytosolic release machinery and/or depletion of the intracellular stores following cell dissociation. It highlights the importance of investigating Ca^{2+} dynamics under metabolic conditions that approximate more closely the *in vivo* situation.

Our recordings, conducted under symmetric $[Cl^-]$ conditions, made it impossible to maintain *effective* holding potentials more negative than about −20 mV (except when using octanol to uncouple cells, thus reducing the input conductance). It is therefore tempting to extrapolate from our present findings and hypothesise that, under transient physiological stresses, ATP would enhance Cl^- permeability at the surface of the organ of Corti increasing anion efflux into the endolymph. Such a movement of Cl^- is likely to promote an equivalent efflux of K^+ through apical membrane channels preserving the electroneutrality of the endolymphatic fluid. This mechanism might contribute to the homeostasis of K^+, facilitating its re-absorption into the endolymph.

Modulation of gap junction conductance

There is increasing evidence that gap junctions, which allow exchange of electrolyte second messengers and metabolites (Bruzzone *et al.* 1996), play a fundamental role in the organ of Corti. For example, the connexins Cx26, Cx30 and Cx31 are all present in the supporting cells of the organ of Corti (A. Forge, personal communication), as well as in the spiral limbus, the spiral ligament and the stria vascularis. Cx26 is thought to be a predominant isoform in the organ of Corti of the cochlea (Forge *et al.* 1999). Mutations in the gene encoding Cx26 (GJB2) cause non-syndromic recessive and dominant forms of deafness (Kelsell *et al.* 1997; Zelante *et al.* 1997; Denoyelle *et al.* 1998). Cx30 (Grifa *et al.* 1999), Cx31 (Xia *et al.* 1998) and Cx32 (Stojkovic *et al.* 1999) have also been implicated in deafness.

Our fluorescence imaging and (double) patch-clamp recordings provide corroborating functional evidence for intercellular coupling within the network of Hensen's cells, mediated by gap junctions with a molecular cut-off size between 0.5 and 1 kDa. The distributed nature of the InsP_3-dependent $[Ca^{2+}]_i$ elevation (Fig. 5*A* and *B*) correlates well with the diffused anti-InsP_3 antibody immunofluorescence and electron microscopy of the ER in these cells (Fig. 6) and indicates a potential for depressing efficiently the conductance of all junctions in a given cell. Depression of electrical coupling following ATP stimulation and/or elevation of the $[Ca^{2+}]_i$ (Fig. 8) indicates that Hensen's cells are capable of co-ordinated cellular activity, potentially exerting a protective control in the presence of certain sustained deleterious stimuli, such as ischaemia or prolonged exposure to high sound pressure levels.

When perfused through scala tympani of the guinea-pig cochlea, ^{14}C-palmitic acid has been shown by auto-radiography to localise primarily to the lipid globules of Hensen's cells and secondarily in the hair cells and the myelin of the cochlear nerve (Tachibana & Takada, 1987). The lipid deposits of the Hensen's cells contain triglycerides, cholesterol esters and two phospholipids species, sphingomyelin and cephalin (Schiff & Christiensen-Lou, 1967). Thus, in principle, they might be the site of intense synthesis and degradation of triglycerides and phospholipids. Ca^{2+} is a well-known activator of lipolysis and stimulates both triglyceride lipases and phospholipases (Arrese *et al.* 1999). This lipolytic activity may potentially release non-esterified fatty acids, as well as arachidonic acid, that are capable of closing intercellular channels in several cell types, possibly during pathophysiological conditions (Bruzzone *et al.* 1996). Cx26, the most abundant type of connexin in Hensen's cells (Forge *et al.* 1999), does not have consensus sequences for kinases, and is not phosphorylated by protein kinase A, protein kinase C or Ca^{2+}–calmodulin protein kinase II (Bruzzone *et al.* 1996). By exclusion, lipophilic compounds thus seem to be one of the possible signals for the gating of gap junctions in Hensen's cells.

Arrese, E. L., Flowers, M. T., Gazard, J. L. & Wells, M. A. (1999). Calcium and cAMP are second messengers in the adipokinetic hormone-induced lipolysis of triacylglycerols in Manduca sexta fat body. *Journal of Lipid Research* **40**, 556–564.

Ashmore, J. F. & Balme, E. J. (1988). Chloride channels in the apical membrane of isolated Hensen cells of the guinea-pig cochlea. *Journal of Physiology* **401**, 97*P*.

Bruzzone, R., White, T. W. & Paul, D. L. (1996). Connections with connexins: the molecular basis of direct intercellular signaling. *European Journal of Biochemistry* **238**, 1–27.

Chessell, H. P., Michel, A. D. & Humphrey, P. P. A. (1997). Properties of the pore-forming $P2X_7$ purinoceptor in mouse NTW8 microglial cells. *British Journal of Pharmacology* **121**, 1429–1437.

Cockcroft, S. & Gomperts, B. D. (1979). Activation and inhibition of calcium-dependent histamine secretion by ATP ions applied to rat mast cells. *Journal of Physiology* **296**, 229–243.

Denoyelle, F., Lina-Granade, G., Plauchu, H., Bruzzone, R., Chaib, H., Levi-Acobas, F., Weil, D. & Petit, C. (1998). Connexin 26 gene linked to a dominant deafness. *Nature* **393**, 319–320.

Dubyak, G. R. & el Moatassim, C. (1993). Signal transduction via P2-purinergic receptors for extracellular ATP and other nucleotides. *American Journal of Physiology* **265**, C577–606.

Dulon, D., Moataz, R. & Mollard, P. (1993). Characterization of Ca^{2+} signals generated by extracellular nucleotides in supporting cells of the organ of Corti. *Cell Calcium* **14**, 245–254.

Flock, A., Flock, B., Fridberger, A., Scarfone, E. & Ulfendahl, M. (1999). Supporting cells contribute to control of hearing sensitivity. *Journal of Neuroscience* **19**, 4498–4507.

Forge, A., Becker, D., Casalotti, S., Edwards, J., Evans, W. H., Lench, N. & Souter, M. (1999). Gap junctions and connexin expression in the inner ear. *Novartis Foundation Symposium* **219**, 134–136.

Grifa, A., Wagner, C. A., D'Ambrosio, L., Melchionda, S., Bernardi, F., Lopez-Bigas, N., Rabionet, R., Arbones, M., Monica, M. D., Estivill, X., Zelante, L., Lang, F. & Gasparini, P. (1999). Mutations in GJB6 cause nonsyndromic autosomal dominant deafness at DFNA3 locus. *Nature Genetics* **23**, 16–18.

Hille, B. (1992). *Ionic Channels of Excitable Membranes*, 2nd edn. Sinauer Associates Inc., Sunderland, MA, USA.

Housley, G. D., Kanjhan, R., Raybould, N. P., Greenwood, D., Salih, S. G., Jarlebark, L., Burton, L. D., Setz, V. C., Cannell, M. B., Soeller, C., Christie, D. L., Usami, S., Matsubara, A., Yoshie, H., Ryan, A. F. & Thorne, P. R. (1999). Expression of the $P2X_2$ receptor subunit of the ATP-gated ion channel in the cochlea: implications for sound transduction and auditory neurotransmission. *Journal of Neuroscience* **19**, 8377–8388.

Kelsell, D. P., Dunlop, J., Stevens, H. P., Lench, N. J., Liang, J. N., Mueller, R. F. & Leigh, I. M. (1997). Connexin 26 mutations in hereditary non syndromic sensorineural deafness. *Nature* **387**, 80–83.

Kikuchi, T., Kimura, R. S., Paul, D. L. & Adams, J. C. (1995). Gap junctions in the rat cochlea: immunohistochemical and ultrastructural analysis. *Anatomical Embryology* **191**, 101–118.

Kirk, D. L. & Yates, G. K. (1998). ATP in endolymph enhances electrically-evoked oto-acoustic emissions from the guinea pig cochlea. *Neuroscience Letters* **250**, 149–152.

Kurahashi, T. & Yau, K. W. (1993). Co-existence of cationic and chloride components in odorant-induced current of vertebrate olfactory cells. *Nature* **363**, 71–74.

Lautermann, J., ten Cate, W. J., Altenhoff, P., Grümmer, R., Traub, O., Frank, H., Jahnke, K. & Winterhager, E. (1998). Expression of the gap-junction connexins 26 and 30 in the rat cochlea. *Cell Tissue Research* **294**, 415–420.

Linden, J. M. (1999). Purinergic systems. In *Basic Neurochemistry: Molecular, Cellular and Medical Aspects*, ed. Siegel, G. J., Agranoff, B. W., Albers, R. W., Fisher, S. K. & Uhler, M. D., pp. 347–362. Lippincott-Raven, Philadelphia.

Lischka, F. W., Zviman, M. M., Teeter, J. H. & Restrepo, D. (1999). Charaterization of inositol-1,4,5-trisphosphate-gated channels in the plasma membrane of rat olfactory neurons. *Biophysical Journal* **76**, 1410–1422.

Mammano, F., Canepari, M., Capello, G. I. R. B., Cunei, A., Ying, L., Fratnik, F. & Colavita, A. (1999*a*). An optical recording system based on a fast CCD sensor for biological imaging. *Cell Calcium* **25**, 115–123.

Mammano, F., Frolenkov, G. I., Lagostena, L., Belyantseva, I. A., Kurc, M., Dodane, V., Colavita, A. & Kachar, B. (1999*b*). ATP-induced Ca^{2+} release in cochlear outer hair cells: localization of an inositol triphosphate-gated Ca^{2+} store to the base of the sensory hair bundle. *Journal of Neuroscience* **19**, 6918–6929.

Mammano, F., Goodfellow, S. J. & Fountain, E. (1996). Electrophysiological properties of Hensen's cells investigated in situ. *NeuroReport* **7**, 537–542.

Merchan, M. A., Merchan, J. A. & Ludena, M. D. (1980). Morphology of Hensen's cells. *Journal of Anatomy* **131**, 519–523.

Muñoz, D. J., Thorne, P. R. & Housley, G. D. (1999). P2X receptor-mediated changes in cochlear potentials arising from exogenous adenosine 5′-triphosphate in endolymph. *Hearing Research* **138**, 56–64.

Nilius, B., Sehrer, J., Heinke, S. & Droogmans, G. (1995). Ca^{2+} release and activation of K^+ and Cl^- currents by extracellular ATP in distal nephron epithelial cells. *American Journal of Physiology* **269**, C376–384.

Oesterle, E. C. & Dallos, P. (1990). Intracellular recordings from supporting cells in the guinea pig cochlea: DC potentials. *Journal of Neurophysiology* **64**, 617–636.

Orkand, R. K. (1986). Introductory remarks: Glial-interstitial fluid exchange. *Annals of the New York Academy of Sciences* **481**, 269–272.

Rose, B., Simpson, I. & Loewenstein, W. R. (1977). Calcium ion produces graded changes in permeability of membrane channels in cell junction. *Nature* **267**, 625–627.

Santos-Sacchi, J. (1987). Electrical coupling differs in the in vitro and in vivo organ of Corti. *Hearing Research* **25**, 227–232.

Schiff, M. & Christiensen-Lou, H. (1967). The nature of lipid globules in Hensen's cells. *Annals of Otology, Rhinology and Laryngology* **76**, 624–637.

Stojkovic, T., Latour, P., Vandenberghe, A., Hurtevent, J. F. & Vermersch, P. (1999). Sensorineural deafness in X-linked Charcot-Marie-Tooth disease with connexin 32 mutation (R142Q) *Neurology* **52**, 1010–1014.

Strauss, O., Steinhausen, K., Mergler, S., Stumpff, F. & Wiederholt, M. (1999). Involvement of protein tyrosine kinase in the InsP3-induced activation of Ca^{2+}-dependent Cl^- currents in cultured cells of the rat retinal pigment epithelium. *Journal of Membrane Biology* **169**, 141–153.

Sugasawa, M., Erostegui, C., Blanchet, C. & Dulon, D. (1996). ATP activates a cation conductance and Ca^{2+}-dependent Cl^- conductance in Hensen cells of guinea pig cochlea. *American Journal of Physiology* **271**, C1817–1827.

Tachibana, M. & Takada, A. (1987). Incorporation of palmitic acid in the organ of Corti as revealed by autoradiography. *Hearing Research* **25**, 121–124.

Thorne, P. R., Muñoz, D. J. B., Housley, G. D., Vlajkovic, S., Kendrick, I. S. & Rasam, M. (1999). Regulation of cochlear sensitivity by extracellular ATP. *Abstracts of the Association for Research in Otolaryngology* 482.

Venance, L., Stella, N., Glowinski, J. & Giaume, C. (1997). Mechanisms involved in initiation and propagation of receptor-induced calcium signalling in cultured rat astrocytes. *Journal of Neuroscience* **17**, 1981–1992.

Vlajkovic, S. M., Thorne, P. R., Housley, G. D., Muñoz, D. J. B. & Kendrick, I. S. (1998). Ecto-nucleotidases terminate purinergic signalling in the cochlear endolymphatic compartment. *NeuroReport* **9**, 1559–1565.

Wangemann, P. (1996). Ca^{2+}-dependent release of ATP from the organ of Corti measured with a luciferin-luciferase bioluminescence assay. *Auditory Neuroscience* **2**, 187–192.

Wangemann, P. & Schacht, J. (1996). Homeostatic mechanisms in the cochlea. In *The Cochlea*, ed. Dallos, P., Popper, A. & Fay, R., pp. 130–185. Springer-Verlag, New York.

White, P. N., Thorne, P. R., Housley, G. D., Mockett, B., Billett, T. E. & Burnstock, G. (1995). Quinacrine staining of marginal cells in the stria vascularis of the guinea-pig cochlea: a possible source of extracellular ATP? *Hearing Research* **90**, 97–105.

Xia, J. H., Liu, C. Y., Tang, B. S., Pan, Q., Huang, L., Dai, H. P., Zhang, B. R., Xie, W., Hu, D. X., Zheng, D., Shi, X. L., Wang, D. A., Xia, K., Yu, K. P., Liao, X. D., Feng, Y., Yang, Y. F., Xiao, J. Y., Xie, D. H. & Huang, J. Z. (1998). Mutations in the gene encoding gap junction protein beta-3 associated with autosomal dominant hearing impairment. *Nature Genetics* **20**, 370–373.

Zelante, L., Gasparini, P., Estivill, X., Melchionda, S., D'Agruma, L., Govea, N., Mila, M., Monica, M. D., Lutfi, J., Shohat, M., Mansfield, E., Delgrosso, K., Rappaport, E., Surrey, S. & Fortina, P. (1997). Connexin26 mutations associated with the most common form of non-syndromic neurosensory autosomal recessive deafness (DFNB1) in Mediterraneans. *Human Molecular Genetics* **6**, 1605–1609.

Acknowledgements

This work was supported by grant Progetto di Ricerca Avanzata CADY, Istituto Nazionale di Fisica della Materia; grant no. 9906194385, Ministero dell'Università e della Ricerca Scientifica (to F.M) and the Wellcome Trust. We thank Inna Belyantseva, Caroline Davies and Pat Riordan for help with the microscopy, Richard Chadwick, Rui Curi, Kuni Iwasa, Anna Menini, John G. Nicholls and Tullio Pozzan for critical comments and helpful suggestions.

Corresponding author

F. Mammano: International School for Advanced Studies, via Beirut 2–4, 34014 Trieste, Italy.

Email: mammano@sissa.it